J. Fluid. Mech. (1982), *vol.* 124, *pp.* 347–362
Printed in Great Britain

Calculations of laminar viscous flow over a moving wavy surface

By E. A. CAPONI, B. FORNBERG†, D. D. KNIGHT‡, J. W. McLEAN, P. G. SAFFMAN† AND H. C. YUEN

Fluid Mechanics Department, TRW Defense and Space Systems Group, Redondo Beach, CA 90278

(Received 2 December 1981 and in revised form 28 April 1982)

The steady, laminar, incompressible flow over a periodic wavy surface with a prescribed surface-velocity distribution is found from the solution (via Newton's method) of the two-dimensional Navier–Stokes equations. Validation runs have shown excellent agreement with known analytical (Benjamin 1959) and analytico-numerical (Bordner 1978) solutions for small-amplitude wavy surfaces. For steeper waves, significant changes are observed in the computed surface-pressure distribution (and consequently in the nature of the momentum flux across the interface) when a surface orbital velocity distribution, of the type found in water waves, is included.

1. Introduction

Solutions for the flow over a specified wavy surface are desirable for understanding the process of wave growth under the action of wind and the effect of surface configurations on drag. Owing to the complexity of these problems, which involve the time-dependent, three-dimensional, turbulent, nonlinear, coupled air–water or water–solid medium motion, substantial idealizations have to be made. Solutions for flow over small-amplitude wavy surfaces were obtained by Miles (1957 and later papers), and by Benjamin (1959). In their work, the surface was regarded as a steadily propagating wave of infinitesimal amplitude on a flexible boundary, which introduced a perturbation on the specified mean flow. Assuming steadiness in the reference frame moving with the wave, the corresponding Orr–Sommerfeld equation for the perturbation of the flow could then be solved numerically, and, for certain limits, analytically.

The removal of the infinitesimal-amplitude assumption requires the solution of the full nonlinear Navier–Stokes equations. The present paper presents some numerical solutions of the two-dimensional steady-state Navier–Stokes equations for laminar viscous flow over a specified steady wave profile of arbitrary amplitude and shape, and arbitrary distribution of surface velocities.

2. Governing equations

We consider the two-dimensional, periodic, viscous, incompressible air flow over a periodic wavy surface propagating with constant wave speed c. In a laboratory-fixed coordinate system, the flow is

$$u' = U(y) + \tilde{u}(x' - ct), \quad v' = \tilde{v}(x' - ct), \tag{1}$$

† Present address: Applied Math, California Institute of Technology, Pasadena, CA 91125.

‡ Present address: Mechanical and Aerospace Engineering, Rutgers University, Piscataway, NJ 08854.

and the surface is

$$y = l(x'-ct), \tag{2}$$

where the origin of y is chosen at the mean level of the wave elevation l, and the dependence on x' is periodic with wavelength $\lambda = 2\pi/k$. The velocity of a fluid particle on the surface is defined to be

$$l_t \mathbf{j} + q(x'-ct)\,\mathbf{\hat{s}}, \tag{3}$$

where $\mathbf{j}$ is the unit vector in the vertical direction and $\mathbf{\hat{s}}$ is the unit tangent to the wave surface. The velocity q (periodic in x') measures the tangential velocity, which may be produced by wave-induced orbital motion and wind drift, or otherwise imposed on the boundary. This boundary condition allows different types of physical surfaces; for example, a rigid wavy wall ($q = 0$, $c = 0$), a flexible wavy wall in which fluid particles on the surface move up and down ($q = 0$, $c \neq 0$), or a water wave ($q \neq 0$, $c \neq 0$).

Relative to a coordinate system ($x = x'-ct$) moving with the steady wave, the stream function $\psi(x, y)$ and vorticity ω satisfy

$$\psi_x \omega_y - \psi_y \omega_x + \nu \nabla^2 \omega = 0, \tag{4a}$$

$$\omega + \nabla^2 \psi = 0, \tag{4b}$$

where

$$v = -\psi_x = v', \quad u = \psi_y = u'-c \tag{5}$$

are the velocities in the wave-fixed frame, and ν is the kinematic viscosity.

The boundary conditions at the wave surface $y = l(x)$ are

$$\psi = 0, \quad \mathbf{\hat{n}} \cdot \nabla \psi = q - \frac{c}{\cos\theta} \tag{6}$$

where $\mathbf{\hat{n}}$ is the normal to the interface into the air, and $\tan\theta$ is the slope of the surface. Periodic boundary conditions are imposed in the horizontal direction.

In an unbounded flow, we require $U(y) \sim \kappa y$, $u \sim U(y)-c$, $v \sim 0$, as $y \to \infty$, where κ is the velocity gradient of the undisturbed flow. For the purpose of computation, it is necessary to work in a finite domain, $y < y_T$, and two conditions must be imposed at this artificial boundary. Among possible choices for the upper boundary conditions, it is desirable to impose conditions for which the solution is insensitive to changes in the location of the upper boundary. Our experience indicated that specification of the vorticity and vorticity flux leads to spurious solutions, and a condition on the vertical velocity causes sensitivity to the location of the upper boundary. We have therefore chosen to impose conditions on the horizontal velocity and the vorticity flux:

$$\psi_y = \kappa y_T - c, \quad \omega_y = \text{constant}. \tag{7}$$

The value of the vorticity flux at the top boundary is determined by the requirement that the pressure be periodic. The adequacy of a chosen value of y_T is determined by requiring that the results are insensitive to increases in y_T.

Another choice for the boundary conditions would be to use the asymptotic form of Benjamin's perturbation solution to formulate a boundary condition; however, it was felt that this correction does not justify the increase in algebraic and computational difficulties. Numerical experience indicates that the boundary condition (7) is a good approximation to the unbounded flow.

It is desirable to perform computations on a fixed rectangular region (independent

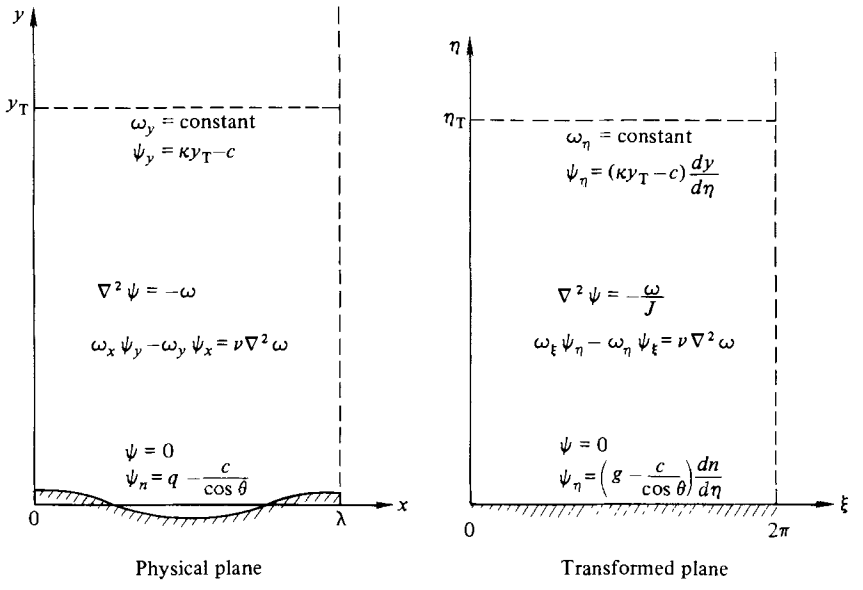

FIGURE 1. Flow geometry: physical and transformed planes.

of the shape of the wavy lower boundary). This was achieved here by the use of the orthogonal transformation

$$\frac{x}{\lambda} = \xi + \sum_1^\infty \frac{b_n}{n}\sin n\xi\left\{\frac{\cosh n(\eta_T - \eta)}{\sinh n\eta_T}\right\}, \tag{8a}$$

$$\frac{y}{\lambda} = \eta + b_0 - \sum_1^\infty \frac{b_n}{n}\cos n\xi\left\{\frac{\sinh n(\eta_T - \eta)}{\sinh n\eta_T}\right\} \tag{8b}$$

to map the physical space under consideration onto the rectangular region $0 \leqslant \xi \leqslant 2\pi$, $0 \leqslant \eta \leqslant \eta_T$, where $\eta_T = y_T/\lambda - b_0$ (see figure 1). The coefficients b_n can be chosen to approximate any given periodic and symmetrical surface. An asymmetric surface can be accommodated by an appropriate modification of (8).

Upon applying the orthogonal transformation, the equations to be solved are

$$\psi_{\xi\xi} + \psi_{\eta\eta} = -\frac{\omega}{J}, \tag{9a}$$

$$\omega_\xi\psi_\eta - \omega_\eta\psi_\xi = \nu(\omega_{\xi\xi} + \omega_{\eta\eta}), \tag{9b}$$

where

$$\frac{1}{J} = x_\xi^2 + x_\eta^2. \tag{10}$$

Since the flow is periodic in the horizontal direction, the dependent variables may be expanded as a Fourier series in ξ:

$$\left.\begin{aligned}\psi &= \sum_0^\infty f_n(\eta)\cos n\xi + \sum_1^\infty g_n(\eta)\sin n\xi,\\ \omega &= \sum_0^\infty s_n(\eta)\cos n\xi + \sum_1^\infty t_n(\eta)\sin n\xi.\end{aligned}\right\} \tag{11}$$

We further expand the Jacobian of the transformation:

$$\frac{1}{J} = \sum_0^\infty h_n(\eta)\cos n\xi. \tag{12}$$

Substituting the expansions into (9*a*, *b*), and equating Fourier components, yields a set of coupled nonlinear ordinary differential equations. Equation (9*a*) becomes

$$\sum_{i=1}^{\infty} i\{-(s_i g_i' + s_i' g_i) + (t_i f_i' + t_i' f_i)\} = 2\nu s_0'' \quad \text{(constant term)}, \tag{13a}$$

$$\begin{aligned}\sum_{i=1}^{\infty} \{&-is_i(g'_{n+i} + \operatorname{sign}(n-i)\, g'_{|n-i|}) + it_i(f'_{n+i} + f'_{|n-i|}) \\ &- s_i'[(n+i)\, g_{n+i} + |n-i|\, g_{|n-i|}] + t_i'[(n+i) f_{n+i} + (n-i) f_{|n-i|}]\} \\ &+ nt_n f_0' - 2ns_0' g_n = 2\nu(s_n'' - n^2 s_n) \quad (\cos n\xi \text{ term}),\end{aligned} \tag{13b}$$

$$\begin{aligned}\sum_{i=1}^{\infty} \{&is_i(f'_{n+i} - f'_{|n-i|}) + it_i(g'_{n+i} - \operatorname{sign}(n-i)\, g'_{|n-i|}) \\ &+ s_i'[(n+i) f_{n+i} - (n-i) f_{|n-i|}] + t_i'[(n+i) g_{n+i} - |n-i|\, g_{|n-i|}]\} \\ &- ns_n f_0' + 2ns_0' f_n = 2\nu(t_n'' - n^2 t_n) \quad (\sin n\xi \text{ term}).\end{aligned} \tag{13c}$$

Equation (9*b*) becomes

$$f_0'' = -\frac{1}{2}\left\{\sum_0^{\infty} h_i s_i + h_0 s_0\right\} \quad \text{(constant term)}, \tag{14a}$$

$$f_n'' - n^2 f_n = -\frac{1}{2}\left\{\sum_0^{\infty} s_i(h_{n+i} + h_{|n-i|}) + s_n h_0\right\} \quad (\cos n\xi \text{ term}), \tag{14b}$$

$$g_n'' - n^2 g_n = -\frac{1}{2}\left\{\sum_1^{\infty} t_i(-h_{n+i} + h_{|n-i|}) + t_n h_0\right\} \quad (\sin n\xi \text{ term}), \tag{14c}$$

with $g_0 = t_0 = 0$. A prime denotes differentiation with respect to η.

The pressure is given by

$$\frac{p}{\rho} + \frac{1}{2}\mathbf{v}\cdot\mathbf{v}\Big|_A^B = \int_A^B (\mathbf{v}\times\boldsymbol{\omega} - \nu\nabla\times\boldsymbol{\omega})\cdot d\mathbf{s} \tag{15}$$

where $\mathbf{v} = (u, v, 0)$, $\boldsymbol{\omega} = (0, 0, \omega)$. Integrating along a constant-η curve, we obtain

$$\frac{p}{\rho} + \frac{1}{2}\mathbf{v}\cdot\mathbf{v}\Big|_0^{\xi} = -\int_0^{\xi} (\omega\psi_\xi + \nu\omega_\eta)\, d\xi. \tag{16}$$

The total horizontal force on the surface is given by

$$F_x = \int (p\sin\theta - \rho\nu\omega\cos\theta)\, ds, \tag{17}$$

where the integration is over one wave period. The non-dimensional pressure and viscous drag coefficients are defined by

$$C_p = \frac{\frac{1}{\lambda}\int p\sin\theta\, ds}{\left(\frac{\nu}{\kappa\lambda^2}\right)\rho(\lambda\kappa)^2}, \quad C_\nu = \frac{-\frac{\rho\nu}{\lambda}\int \omega\cos\theta\, ds}{\left(\frac{\nu}{\kappa\lambda^2}\right)\rho(\lambda\kappa)^2}. \tag{18}$$

The normalization is chosen so that $C_\nu = 1$ for a flat interface.

A further condition on the flow is that the pressure be periodic, yielding the condition

$$\int_0^{2\pi} (\omega\psi_\xi + \nu\omega_\eta)\, d\xi = 0 \quad \text{on} \quad \eta = \text{constant}. \tag{19}$$

Evaluating this integral at $\eta = \eta_T$ leads to an equation for the value of the constant vorticity flux. The complete set of boundary conditions becomes

$$\left.\begin{aligned} f_n(0) = g_n(0) &= 0, \\ \left.\begin{matrix} f_n'(0) \\ g_n'(0) \end{matrix}\right\} &= n\text{th Fourier component of } \left(q - \frac{c}{\cos\theta}\right) J^{-\frac{1}{2}}, \\ \left.\begin{matrix} f_n'(\eta_T) \\ g_n'(\eta_T) \end{matrix}\right\} &= n\text{th Fourier component of } (\kappa y_T - c)\frac{dy}{d\eta}, \\ s_n'(\eta_T) = t_n'(\eta_T) &= 0 \quad (n \neq 0), \\ s_0'(\eta_T) &= -\frac{1}{2\nu}\sum_1^\infty n(s_n g_n - t_n f_n)|_{\eta=\eta_T}. \end{aligned}\right\} \tag{20}$$

This completes the specification of the problem.

In the numerical computations, an explicit stretching in the vertical direction is introduced to resolve boundary layers. The stretching $\zeta(\eta)$ defined by

$$\eta = \eta_T \frac{e^{b\zeta} - 1}{e^b - 1}, \tag{21}$$

with values of b ranging from 1 to 10, was found to provide adequate resolution.

3. Method of solution

The set of equations (13) and (14) is discretized on a uniform mesh on $0 \leqslant \zeta \leqslant 1$ using centred differences for the derivatives. The expansion (11) is truncated at N Fourier modes, that is, we take f_n, g_n, s_n, t_n to be zero for $n > N$ in the equations. As primary unknowns, we take the values of $\{s_n, t_n\}$ at $\zeta = 0, \Delta, 2\Delta, \ldots, 1-\Delta$ ($\Delta = (M+1)^{-1}$). From (14) at $\zeta = 0, \Delta, \ldots, 1-\Delta$, we can solve for $\{f_n, g_n\}$ at $\zeta = \Delta, 2\Delta, \ldots, 1$ in terms of the primary unknowns. Equation (14) at $\zeta = 1$ gives $\{s_n(1), t_n(1)\}$ as functions of the primary unknowns. Using these relations, (13) at $\zeta = \Delta, 2\Delta, \ldots, 1$ gives $(2N+1)(M+1)$ equations for the $(2N+1)(M+1)$ unknowns $\{s_n, t_n\}$ at $\zeta = 0, \Delta, \ldots, 1-\Delta$. This nonlinear system is solved by Newton's method.

Several tests are imposed to determine whether the mesh spacing and Fourier truncation is adequate to resolve details of the flow. At the top boundary, $\zeta = 1$, the pressure is constrained to be periodic, and thus must be periodic for all values of ξ. Evaluating (19) at $\zeta = 0$ is one indication of the resolution of the finite mesh. For the data presented here, the pressure difference between $\xi = 0$ and $\xi = 2\pi$ was less than 1 % of the peak-to-peak pressure. To test overall momentum conservation for the numerical solution, the horizontal force plus the horizontal component of the momentum flux at the upper surface can be compared with the drag at the surface. Numerical solutions were rejected if the discrepancy was greater than 2 %.

Some of the results presented here had been previously calculated (Caponi 1979) using a successive-iteration approach. In that case, the steady state was obtained as the asymptotic temporal limit of the parabolic equations that model the parabolic–elliptic set of real time-dependent equations for the stream function and vorticity.† It is well known that for such an approach the solution process can become quite lengthy, being very sensitive to the treatment of the lower boundary condition on the vorticity. Although selected runs on small-size meshes demonstrated that the

† Time stepping was done with a modified ADI algorithm.

method converged to a solution of the steady-finite-difference equations, computational economics dictated the need to establish 'convergence criteria' to allow for the acceptance of still evolving fields as the converged steady solution. The results so obtained compared well with solutions for special cases found by independent methods, and served to validate the criteria used for determining convergence. However, the overall efficiency of the pseudo-time-dependent method was not satisfactory.

Part of the poor convergence properties of that approach can be attributed to using successive iterations for the stream function ψ and the vorticity ω with the cycle closed by manufacturing a value for the vorticity at the lower boundary from the no-slip condition for the stream function. This is a consequence of the fact that the physical boundary conditions overspecify ψ and underspecify ω. Such a situation does not arise when one solves simultaneously for ψ and ω, as is the case of the present approach. When using Newton's method, convergence is quadratic, and running times in this case are substantially accounted for by the time spent in matrix inversion. A further characteristic of using Newton's method for a steady solution is that convergence is independent of the hydrodynamic stability of the flow. Although the Jacobian matrix has substantial zero structure, for ease of computation we treated the matrix as full, with resulting penalties in running times and storage requirements.

4. Results

The properties of the flow field depend on a number of parameters. For a wave of given form (e.g. a sinusoid or Stokes wave), the surface is specified by its wavelength λ, peak-to-trough height h, and speed c. In addition, the flow field depends on the imposed shear κ, the kinematic viscosity ν, and a distribution of surface tangential velocity q. It is convenient to introduce three dimensionless parameters: the Reynolds number $R = U_\lambda \lambda/\nu$, where $U_\lambda = \kappa\lambda$ is the undisturbed flow speed at $y = \lambda$; the wave slope h/λ; and a 'wave age' c/U_λ.

For $c/U_\lambda > 0$, there is a critical layer at a height $y_c = \lambda c/U_\lambda$, where the undisturbed flow speed is equal to the speed of the wave, and there are regions of closed streamlines in a wave-fixed coordinate system (cat's-eyes). At large Reynolds number, there is an internal boundary layer about y_c, called the friction layer, whose thickness is given by $\delta_F = \lambda R^{-\frac{1}{3}}$ when the amplitude of the motion is not too large (Benney & Bergeron 1968). The computational domain must be large enough to contain the friction layer, and experience indicated that choosing y_T to be some multiple of δ_F (10–20 typically) was sufficient to approximate the unbounded flow for our range of R and y_c.

A rigid wavy surface corresponds to $q = 0$ and $c = 0$. Non-zero values of c with $q = 0$ corresponds to a flexible boundary along which a wave is propagating while the particles on the surface move up and down. A water wave is a flexible boundary with non-zero q composed of wave-induced orbital velocity and possibly a wind drift. In the absence of wind drift, and assuming irrotational flow, the wave-induced tangential velocity can be obtained from the Bernoulli condition for the Stokes wave:

$$q^2 = c^2 - 2gl(x) \tag{22}$$

where $l(x)$ is the elevation of the wave surface, c is the phase speed of the wave ($(g\lambda/2\pi)^{\frac{1}{2}}$ for an infinitesimal wave), and g is the acceleration due to gravity.

Solutions for small values of h/λ and $q = 0$ were generated for various values of

c for the purpose of comparing with Benjamin's (1959) linear analysis. His asymptotic linear theory result for large Reynolds number is

$$\frac{p}{\rho U_\lambda^2} = -\pi\left(\frac{h}{\lambda}\right)\alpha(1-\alpha z_0)\{A_c(\cos u - 1) + A_s \sin u\}, \tag{23}$$

where

$$\alpha = \left(\frac{4\pi^2}{R}\right)^{\frac{1}{3}}, \quad z_0 = (2\pi)^{\frac{1}{3}}\left(\frac{y_c}{\delta_F}\right),$$

$$A_s = -D_i[1+\alpha(2D_r - z_0)],$$

$$A_c = (D_r - z_0)(1+\alpha D_r) - \alpha D_i^2,$$

$$u = 2\pi\left(x + \tfrac{1}{2}h\sin\frac{2\pi x}{\lambda}\right)/\lambda.$$

D_r and D_i are the real and imaginary parts of the Tietjens function evaluated at $-z_0$. The linearization requires

$$\frac{h}{\delta_F} \ll \frac{\delta_F}{y_c} \tag{24}$$

if $y_c/\delta_F \gg 1$ (Benney & Bergeron 1968), or

$$\left(\frac{h}{\delta_F}\right)^2 \ll 1 \tag{25}$$

if $y_c/\delta_F \leqslant O(1)$ (Bordner 1978) (see appendix). Figure 2 presents plots of p versus x on the surface for $y_c/\delta_F = 10$, $h/\lambda = 0{\cdot}001$, with (*a*) $y_c h/\delta_F^2 = 0{\cdot}22$ ($R = 10^4$) and (*b*) $y_c\,h/\delta_F^2 = 1{\cdot}0$ ($R = 10^6$). In figure 3, results are shown for $y_c/\delta_F = 0$, $R = 10^6$, and (*a*) $h/\lambda = 10^{-3}$, (*b*) 10^{-2}, (*c*) 2×10^{-2}, corresponding to $(h/\delta_F)^2 = 0{\cdot}01$, $1{\cdot}0$, 4. These results serve to validate the numerical procedures (figures 2*a*, 3*a*) and show clearly that the failure of the linear theory when (24) or (25) is violated (figures 2*b*, 3*b*, 3*c*).

The pressure-drag coefficient, defined by (18), depends on both the amplitude and phase of the surface-pressure distribution. The phase will be defined as $\theta = 2\pi x_m/\lambda$, where x_m is the location where the pressure is at a maximum. Note that the crest of the wave is always taken to be $x = 0$. For the linear theory, the pressure-drag coefficient is quadratic in h/λ owing to the linear dependence of pressure amplitude and wave slope on h/λ. The dependence on R and c/U_λ is more subtle, and enters through both the amplitude and the phase, with the major effect being through the phase. For instance, the result that $C_p < 0$ for $c/U_\lambda < 0$ or $c/U_\lambda > 0$ and large is a consequence of the phase shifting owing to changes in c/U_λ.

We now investigate the effects of wave nonlinearity. The surface in all calculations is taken to be that of a Stokes wave of height h. The tangential velocity is either zero or that corresponding to the Stokes wave, with or without an additional wind-drift contribution.

We first plot in figures 4 and 5 the ratio of the pressure to viscous drag versus wave steepness for two values of Reynolds number (4×10^4 and 10^2), and four values of c/U_λ ($-1{\cdot}46\times10^{-2}$, $2{\cdot}92\times10^{-3}$, $1{\cdot}46\times10^{-2}$ and $5{\cdot}85\times10^{-2}$) with and without orbital velocity, and without wind drift.

The departure from linear theory with increasing wave amplitude is a result of three effects: (i) departure from the linear growth of the peak-to-peak pressure; (ii) variation in the phase of the pressure distribution; and (iii) contributions from higher harmonics of the pressure distribution. For the parameter range of our computations, the last effect on the pressure drag coefficient is found by direct computation to be negligible.

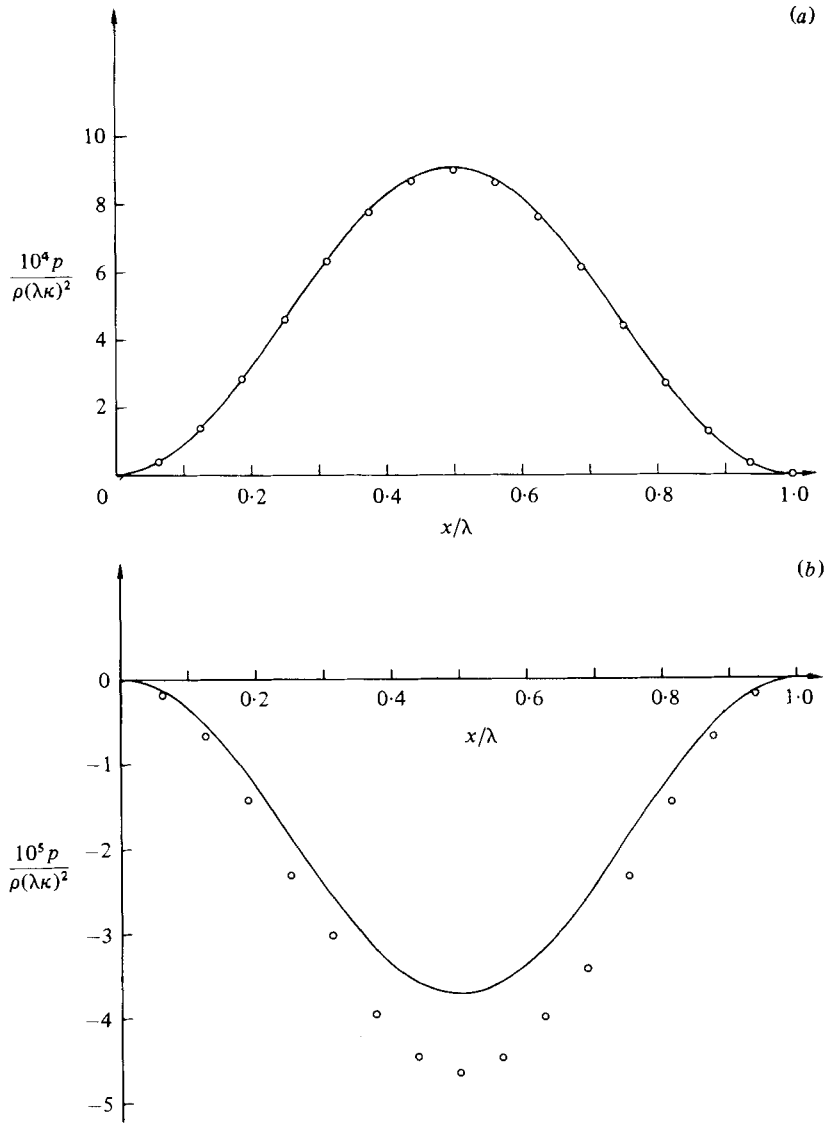

FIGURE 2. Wall-pressure distribution; $y_c/\delta_F = 10{\cdot}0$, $h/\lambda = 0{\cdot}001$: ——, linear theory; ○, numerical solution. (*a*) $hy_c/(\delta_F)^2 = 0{\cdot}215$; (*b*) 1·0.

For the case of the larger Reynolds number ($R = 4 \times 10^4$, figure 4), it is found from detailed examination of the results that the amplitude of the pressure increases slower than linear as the wave steepness increases. This effect is more pronounced for the adverse-wind case (figure 4*a*), and the smallest-positive-wind case (figure 4*b*); in these cases the pressure amplitude for $h/\lambda = 0{\cdot}05$, say, is about one-half that of the linear theory. For the higher-wave-speeds cases (figures 4*c*, *d*) it is approximately 90%. In all these cases, the effect of the orbital velocity on the pressure amplitude is small. The effect of finite amplitude on the phase distribution is found to move the phase towards zero, i.e. to lock the pressure distribution and surface elevation in phase. If the phase is initially more than 90° away from the crest, this generally leads to an enhancement in the pressure coefficient, as the increase in the phase contribution when the phase is in the vicinity of 90% more than balances the

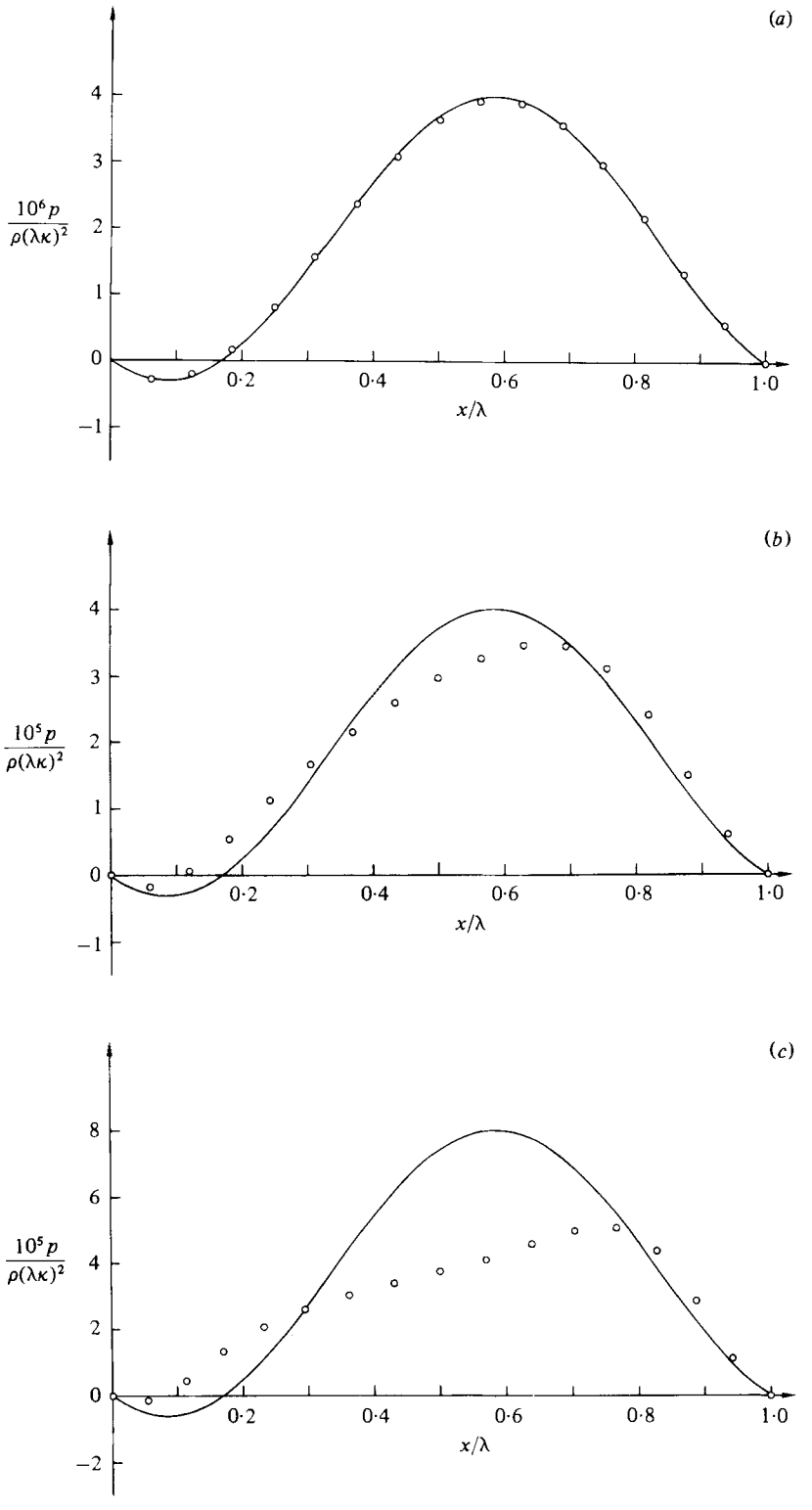

FIGURE 3. Wall-pressure distribution; $y_c/\delta_F = 0, R = 10^6$: ——, linear theory; ○, numerical solution. (*a*) $(h/\delta_F)^2 = 0{\cdot}01$; (*b*) 1; (*c*) 4.

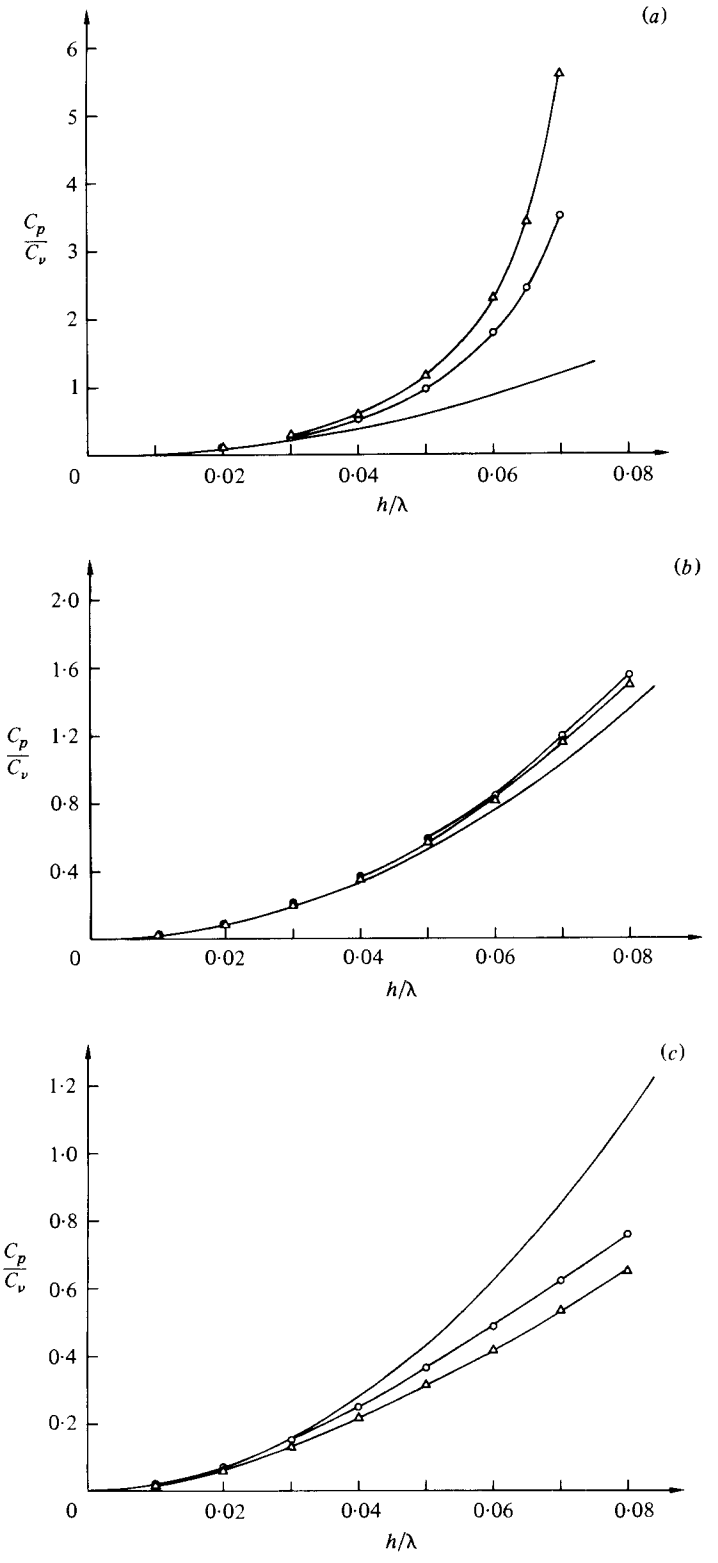

FIGURE 4. For caption see facing page.

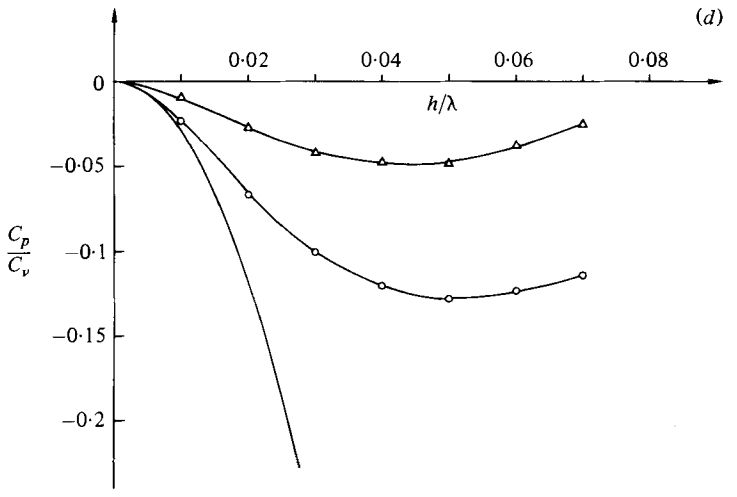

FIGURE 4. Ratio of pressure- to viscous-drag coefficients, showing finite-amplitude effect; $R = 4 \times 10^4$: ——, linear theory (equation (25)); △, numerical solution with orbital velocity; ○, without orbital velocity. (*a*) $c/U_\lambda = -0{\cdot}015$; (*b*) 0·003; (*c*) 0·015; (*d*) 0·058.

reduction of the amplitude of the pressure from the linear value. This is the explanation of the results shown in figures 4 (*a*, *b*). When the phase is initially less than 90% away from the crest, the nonlinearity-induced shift of the phase causes a reduction in the absolute magnitude of the drag coefficient as seen in figures 4 (*c*, *d*). Also, the orbital velocity is found to have only a minute effect on the phase.

For the case of the lower Reynolds number ($R = 100$), the situation is completely different. In almost every case, it is found that the phase is practically independent of the wave height, with or without orbital velocity. All the departures from the predictions of the linear theory result from dependence of the pressure amplitude on the wave height. In contrast to the high-Reynolds-number case, the pressure amplitude increases with h/λ at a rate greater than linear, with the exception of the fastest-wave case (figure 5*d*), in which the orbital velocity is found to reduce the amplitude compared with linear.

The results summarized in these two sets of figures clearly indicate that there is a subtle and intricate interplay between finite amplitude and viscous effects. It is not clear to us at present how these results can be predicted and understood by simple models and arguments, and this is an area that warrants substantial further research.

5. Modelling the effects of a wind drift

It is well known that the action of wind on water is not only to generate waves but also to induce a surface drift current. The structure of this wind-drift current has been found to be extremely difficult to determine, even by careful and precise measurements (Wu 1975), and has not been studied theoretically in a systematic fashion. Banner & Phillips (1974) proposed a model based on the idealized assumption that the flow is steady and the motion is inviscid outside a thin drift layer. This leads to a tangential velocity given by

$$\tfrac{1}{2}q^2 + gl(x) = \tfrac{1}{2}(c - q_{\mathrm{d0}})^2, \tag{26}$$

where c is the phase speed of an inviscid, irrotational water wave (Stokes wave), and q_{d0} is the drift current at the mean elevation ($l(x) = 0$)†. There is a stagnation point

† Use of this condition was suggested by a referee.

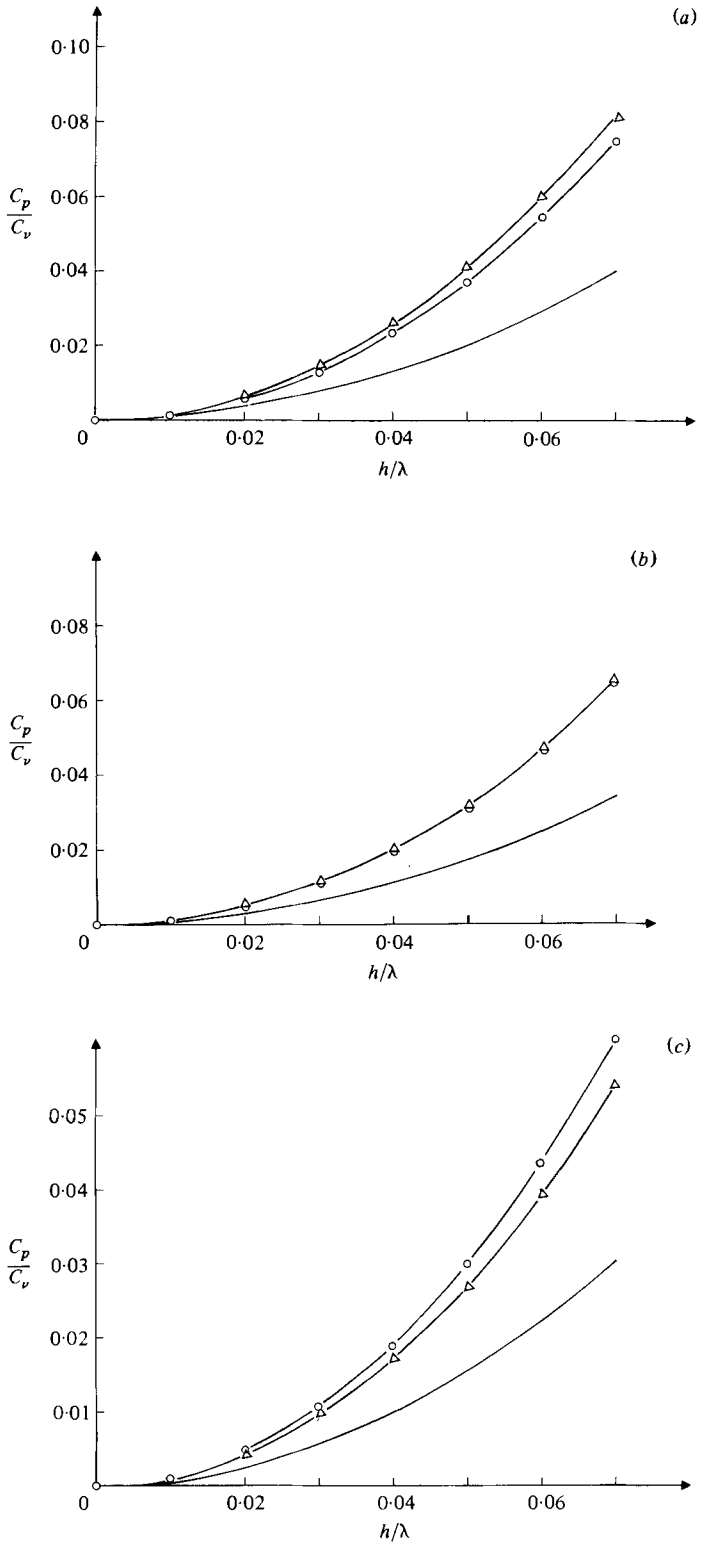

FIGURE 5. For caption see facing page.

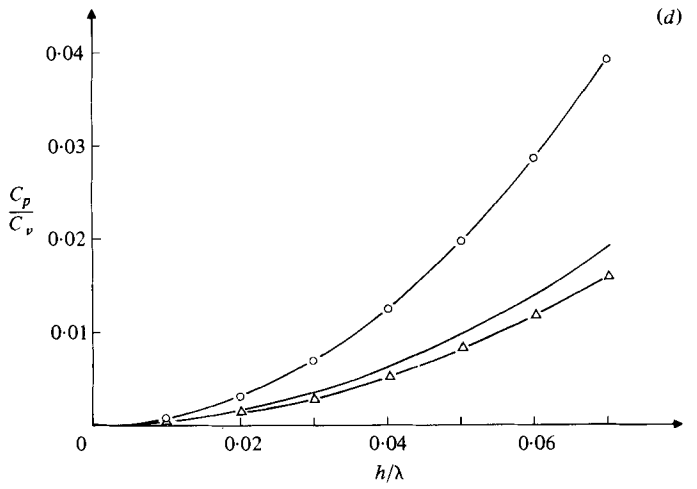

FIGURE 5. Ratio of pressure to viscous drag as in figure 4; $R = 100$.

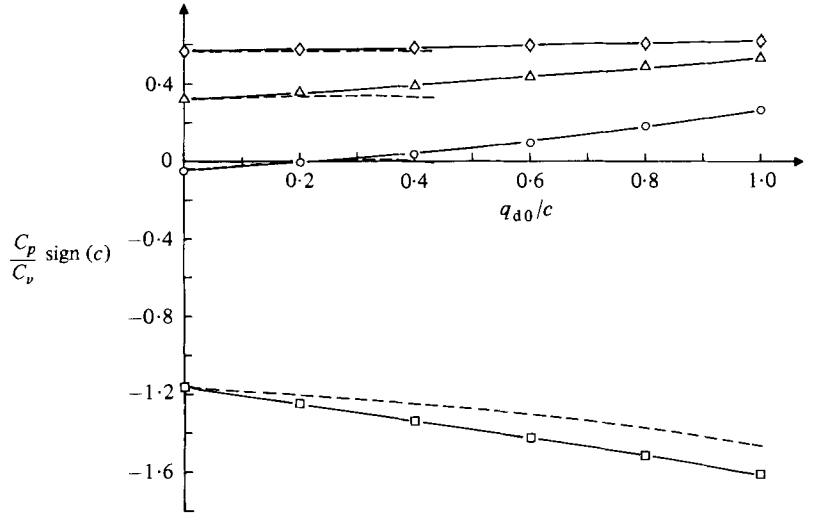

FIGURE 6. Effect of drift velocity on the ratio of pressure to viscous drag; $R = 4 \times 10^4$; $h/\lambda = 0{\cdot}05$: □, $c/U_\lambda = -0{\cdot}015$; ◇, 0·003; △, 0·015; ○, 0·058; ——, simple additive drift (27); – – –, expression (26).

at the crest when $q_{d0} = c - (2gl_{max})^{\frac{1}{2}}$, but the surface-velocity distribution (26) does not allow separated flow. To investigate the effects of separation, we assumed that the surface-velocity distribution to be given by a simple additive drift

$$q = q_{d0} - (c^2 - 2gl(x))^{\frac{1}{2}} \tag{27}$$

For $q_{d0} > (c^2 - 2gl_{max})^{\frac{1}{2}}$ there is a separation bubble in the trough of the wave. Equation (27) is not consistent with the assumption of a steady, nearly irrotational flow in the water (which is itself questionable), but is relevant to the present investigation, which is directed towards the properties of flow over a prescribed surface with general velocity distributions.

The results for $R = 4 \times 10^4$ and $h/\lambda = 0{\cdot}05$ with both wind-drift models are summarized in figure 6, where we have plotted C_p/C_ν as a function of q_{d0}/c for the four values of c/U_λ. The main effects are found to be analogous to a reduction in the

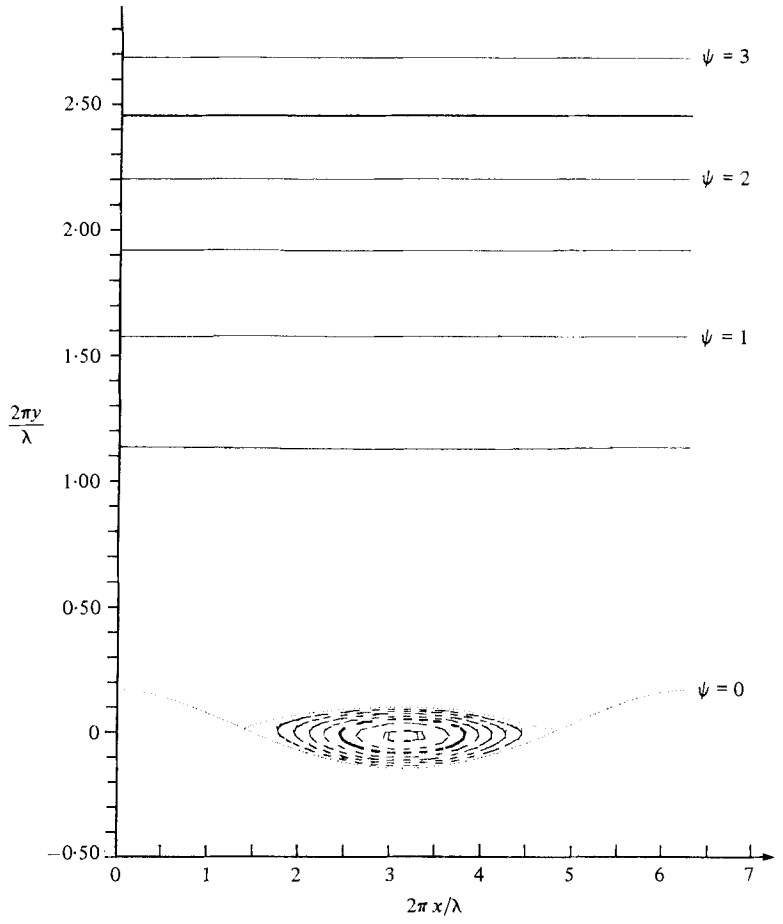

FIGURE 7. Streamline contours showing separation bubble; $R = 4{\cdot}10^4$, $y_c/\delta_F = 0{\cdot}058$, $h/\lambda = 0{\cdot}05$, $q_d/c = 1{\cdot}0$.

wave speed c. In regimes where both models were computed, the results show only small differences. Separated flow occurs for the constant-drift model (equation (27)) when $q_{d0}/c \geqslant 0{\cdot}828$, but no drastic effects in C_p have been detected. An example of the flow field for the case $c/U_\lambda = 0{\cdot}058$ and $q_{d0}/c = 1$ is shown in figure 7.

6. Concluding remarks

We have presented results for steady laminar flow of a viscous fluid over a moving wavy surface, obtained by numerical solution of the unapproximated Navier–Stokes equations, which serve to identify the effects of wave nonlinearity and the surface-velocity distribution. The results provide a basis for studies of instability mechanisms in flow over wavy surfaces and possible ways to delay or accelerate transition. They also constitute a concrete step towards understanding the mechanism of momentum transfer between wind and waves, although for this particular application it is understood that effects of turbulence, unsteadiness of the surface, and viscous effects in the water may also be important, and should be included when considering the full problem. However, by allowing for the existence of a drift layer superposed on the orbital velocity of a Stokes wave, the leading-order effect of a viscous water on the air flow has been accounted for.

This work was partially supported by NSF contract OCE 81-00517, and by TRW internal research and development funds.

Appendix

In this appendix we compare magnitudes of terms in the Navier–Stokes equations to determine the range of validity for linearization in the wave steepness. The steady Navier–Stokes equations are

$$uu_x + vu_y = -p_x + \nu(u_{xx} + u_{yy}), \tag{A 1a}$$

$$uv_x + vv_y = -p_y + \nu(v_{xx} + v_{yy}). \tag{A 1b}$$

The uniform shear flow over a flat surface $(u, v) = (\kappa y - c, 0)$ is perturbed by a periodic wavy deformation of the surface of amplitude h. For an incompressible fluid, small velocity perturbations (u', v') can be expressed in terms of a stream function:

$$u' = \frac{\partial}{\partial y}(\phi(y)\, e^{i2\pi x/\lambda}), \quad v' = -\frac{\partial}{\partial x}(\phi(y)\, e^{i2\pi x/\lambda}).$$

Linearizing in the perturbation leads to the familiar Orr–Sommerfeld equation:

$$(U(y)-c)\left(\phi_{yy} + \left(\frac{2\pi}{\lambda}\right)^2 \phi\right) = i\nu\left(\frac{\lambda}{2\pi}\right)\left(\phi_{yyyy} - 2\left(\frac{2\pi}{\lambda}\right)^2 \phi_{yy} + \left(\frac{2\pi}{\lambda}\right)^4 \phi\right), \tag{A 2}$$

Where $U(y) = \kappa y$. For large Reynolds numbers ($\nu/\kappa\lambda$ small), the right-hand side of (A 2) can be neglected except in the neighbourhood of the critical layer where $U(y) - c = 0$. The critical layer is characterized by large changes in ϕ over a small distance δ_F. Thus the dominant terms in (A 2) are

$$(U-c)\,\phi_{yy} \sim \kappa\delta_F\left(\frac{\phi}{\delta_F^2}\right) \tag{A 3a}$$

$$\nu\lambda\phi_{yyyy} \sim \nu\lambda\left(\frac{\phi}{\delta_F^4}\right), \tag{A 3b}$$

which leads to a balance if $\delta_F = (\nu\lambda/\kappa)^{\frac{1}{3}}$.

Within the critical layer, the neglected nonlinear terms have magnitude $v'u'_y$, thus the linearization requires

$$\frac{v'u'_y}{(U-c)\,u'_x} \sim \frac{v'(u'/\delta_F)}{\kappa\delta_F(u'/\lambda)} \ll 1. \tag{A 4}$$

The deformation at the wall introduces a vertical velocity perturbation of magnitude $v' \sim \bar{U}dy/dx \sim \bar{U}(h/\lambda)$, where $\bar{U}$ is a characteristic horizontal velocity at the wall. If the critical layer is away from the wall ($y_c/\delta_F \gg 1$), then $\bar{U} \sim -c$ and hence $v' \sim c(h/\lambda)$. If the critical layer is at the wall, ($y_c/\delta_F \leqslant O(1)$), the surface distortion introduces a vertical velocity of magnitude $v' \sim \kappa h(h/\lambda)$. Hence neglect of the nonlinear terms requires:

$$\left(\frac{y_c}{\delta_F}\right)\left(\frac{h}{\lambda}\right) \ll \frac{\delta_F}{\lambda} \quad \left(\frac{y_c}{\delta_F} \gg 1\right),$$

$$\left(\frac{h}{\delta_F}\right)^2 \ll 1 \quad \left(\frac{y_c}{\delta_F} \leqslant O(1)\right).$$

REFERENCES

BANNER, M. L. & PHILLIPS, O. M. 1974 On the incipient breaking of small scale waves. *J. Fluid Mech.* **65**, 647–656.

BENJAMIN, T. B. 1959 Shearing flow over a wavy boundary. *J. Fluid Mech.* **6**, 161–205.

BENNEY, D. J. & BERGERON, R. F. 1968 A new class of nonlinear waves in parallel flows. *Stud. Appl. Math* **48**, 181–204.

BORDNER, G. L. 1978 Nonlinear analysis of laminar boundary layer flow over a periodic wavy surface. *Phys. Fluids* **21**, 1471–1474.

CAPONI, E. A. 1979 Laminar air flow over prescribed water waves. *TRW Tech. Rep.* no. 9994–6447-RU-00.

MILES, J. W. 1957 On the generation of surface waves by shear flows. *J. Fluid Mech.* **3**, 185–204.

WU, J. 1975 Wind-induced drift currents. *J. Fluid Mech.* **68**, 49–70.